Romanian Reports in Physics, Vol. 65, No. 1, P. 5–26, 2013

THEORETICAL PHYSICS

PT-SYMMETRIC DOUBLE-WELL POTENTIALS REVISITED: BIFURCATIONS, STABILITY AND DYNAMICS

A. S. RODRIGUES,[1] K. LI,[2] V. ACHILLEOS,[3] P. G. KEVREKIDIS,[2]
D. J. FRANTZESKAKIS,[3] C. M. BENDER[4]

[1] Universidade do Porto, Faculdade de Ciências, Departamento de Física/CFP, R. Campo Alegre, 687 - 4169-007 Porto, Portugal
[2] University of Massachusetts, Department of Mathematics and Statistics, Amherst, MA 01003-9305, USA
[3] University of Athens, Department of Physics, Panepistimiopolis, Zografos, Athens 157 84, Greece
[4] Washington University, Department of Physics, St. Louis, MO 63130, USA

Received December 11, 2012

Abstract. This work presents a two-mode analysis of PT-symmetric double-well potentials. The problem is reduced to a PT-symmetric dimer and it is shown that there are effectively two fundamental bifurcations, a pitchfork bifurcation (symmetry-breaking bifurcation) and a saddle-center bifurcation (nonlinear analog of the PT-phase transition). It is shown that symmetry breaking leads to ghost states, which are associated with growth or decay; although these states are not true solutions of the original continuum problem, the dynamics of the system closely follows them, at least in its metastable evolution. Past the second bifurcation, there are no longer states of the original continuum system. Nevertheless, the solutions can be analytically continued to yield a new pair of branches, which are identified and examined. The explicit analytical results for the dimer are compared directly with the full continuum problem and good agreement is found.

Key words: PT-symmetry, double-well potential, dimmer.

1. INTRODUCTION

PT-symmetric quantum systems [1, 2] have emerged as an intriguing complex generalization of conventional quantum mechanics and have been a focus for numerous investigations at the interface between theoretical physics and applied mathematics. The key premise is that fundamental physical symmetries such as parity P and time reversal T may be sufficient (in suitable parametric regimes) to ensure that the eigenvalues of the Hamiltonian are real. Thus, PT-symmetric Hamiltonians provide an alternative to the standard postulate that the Hamiltonian

operator be Dirac Hermitian (invariant under matrix transposition and complex conjugation *). In the context of Schrödinger Hamiltonians with a complex potential $V(x)$, the constraint of PT symmetry requires that the potential satisfy $V(x)=V^*(-x)$; that is, $V(x)$ has a symmetric real part and an antisymmetric imaginary part.

On the other hand, *nonlinear* Schrödinger (NLS) equations incorporating double-well potentials have received attention due to applications in atomic and optical physics. Such potentials can easily be realized in the context of atomic Bose-Einstein condensates (BECs) through the combination of a parabolic (harmonic) trap with a periodic potential. Experiments have observed fundamental effects, including tunneling and Josephson oscillations for small atom numbers, macroscopic quantum self-trapped states for large atom numbers [3], and nonlinearity-induced symmetry-breaking dynamical instabilities [4]. Theoretical studies accompanying these developments have examined finite-mode reductions, analysis of the bifurcations and their dynamical implications [5–12], as well as quantum effects [13] and nonlinear variants of the potentials [14]. A similar phenomenology has also been found in nonlinear optical settings, with results for the formation of asymmetric states in dual-core fibers [15], self-guided laser beams in Kerr media [16], and optically-induced dual-core waveguide structures in photorefractive crystals [17].

Recently, double-well potentials in the context of PT-symmetric nonlinear systems have received considerable attention. This is due to the pioneering proposal of Ruschhaupt *et al.* and experimental results of Christodoulides and collaborators, who proposed that optics presents a fertile ground for the experimental realization of PT-symmetric systems [18]. The first realization of PT-symmetry in a waveguide coupler arose in the so-called passive-PT setting in which two waveguides, one with loss and the other without loss, were used [18]. A similar proposal for the existence of a leaking dimer (in the presence of nonlinearity) was formulated in the atomic setting of Bose-Hubbard models [19]. Subsequently, an optical waveguide system with both gain and loss was studied and the role of the nonlinearity in the dynamics was explored [20]. Further experimental investigations were concerned with electrical analogs of the system [21]. Theoretical investigations have rapidly followed by examining such dimer-type settings [22–34] and generalizations thereof, including ones where the gain-loss contributions appear in a balanced form in front of the nonlinear term [35–37].

This paper revisits this theme of PT-symmetric double-well potentials. Our motivation is to unify the above studies with an important recent contribution, namely, Ref. [38]. To be specific, in the early works on NLS models with double-well potentials [5, 11, 12, 39], and also in the PT-symmetric dimer [28], the symmetry-breaking bifurcation was identified, but the asymmetric states that

normally accompany the bifurcation [5, 11, 12] could not be identified. The simpler system of a PT-symmetric pair of δ-function potentials, where the solution can be obtained by means of a five-dimensional numerical root search, was studied in Ref. [38]. There, it was found that the bifurcation results in the emergence of what we call a *ghost state*, namely, a solution of the steady-state problem with a *complex* nonlinear eigenvalue parameter (complex propagation constant in optics or complex chemical potential in BECs). [These states were discussed in a 2006 paper for the case of the (discrete) leaking dimer [19].] Another observation of Ref. [38] concerned the possibility of performing an *analytic continuation* of the symmetric and antisymmetric solutions of the original double-well problem *past the point of their PT phase transition*; that is, past the critical point of the saddle-center bifurcation where they disappear simultaneously. This is in the broader spirit of PT-symmetric quantum mechanics [2].

In this paper we study an NLS model with a double-well potential, which has an even real part and a PT-symmetric imaginary part. We combine the above ideas, interweaving analytics based on the two-mode analysis of the simple dimer model and numerics in the framework of the partial differential equation (PDE). There are a number of concurrent works on this theme. In the recent work [40], the static problem of the PT-symmetric dimer is addressed and a Bogolyubov-de Gennes analysis of the relevant states is provided. In the present work, the dimer is used as a tool for understanding the PDE existence and stability problem and, in addition, we examine the dynamics of the obtained states. Another recent work considers the PT-symmetric double-well potential [41]. There, a double well was studied in a functional form similar to the one considered here and with an imaginary part that was also earlier used in Ref. [42]. A time-dependent variational principle was developed (that was ultimately solved numerically) for the three-dimensional case and the full one-dimensional case was also solved numerically. The advantage of the fully analytical results in the present paper is that they provide fundamental qualitative and quantitative insights into the numerical observations of Ref. [41]. In a sense, this work serves as a bridge between the discrete dimer analysis of Ref. [40] and the continuum double-well numerical results of Refs. [38, 41] and offers connections and detailed comparisons between the two.

The paper is organized as follows. We present the two-mode analysis of the discrete nonlinear Schrödinger equation (DNLS) dimer in Sec. 2, where we examine the symmetric/antisymmetric and asymmetric states and the potential for nonlinearity-induced symmetry-breaking bifurcations. We show how the PT-symmetric variant of the dimer problem adjusts these features. The modified critical point of the pitchfork bifurcation is identified, and the feature of a saddle-center bifurcation, which is a nonlinear analog of the PT phase transition, is discussed in the spirit of some of the earlier work on this theme. The key by-products of these bifurcations, namely, the ghost states emanating from the pitchfork and the analytically

continued states past the nonlinear analog of the PT phase transition, are found in *analytical* form. Armed with these analytical results, we study the full PDE problem in Sec. 3, where the aim is to reduce the PDE, through suitable and fully quantified approximations and transformations (so that one can translate the dimer results to the PDE and *vice-ver*sa), to a PT -symmetric dimer. We compare the analytical results concerning the dimer problem with numerical ones obtained in the framework of the original NLS model. In addition to quantifying the bifurcations and identifying their "daughter" states, we examine the dynamics of the various unstable states within the system. Finally, in Sec. 4 we briefly summarize our findings and present some possibilities for further study.

2. DNLS DIMER

2.1. CLASSICAL DNLS DIMER

We begin our exposition by revisiting a simpler initial problem that has been long studied (see, e.g., Ref. [39]), namely the DNLS dimer of the form

$$\begin{aligned} \mathrm{i}\frac{\mathrm{d}u_1}{\mathrm{d}t} &= -ku_2 - |u_1|^2 u_1, \\ \mathrm{i}\frac{\mathrm{d}u_2}{\mathrm{d}t} &= -ku_1 - |u_2|^2 u_2, \end{aligned} \tag{1}$$

where the evolution variable t denotes the propagation distance in optics. As is customary, we seek stationary solutions of the form $u_1 = \exp(\mathrm{i}Et)\ a$ and $u_2 = \exp(\mathrm{i}Et)\ b$, where the complex amplitudes a and b and the propagation constant E are determined by the equations

$$Ea = kb + |a|^2 a, \quad Eb = ka + |b|^2 b. \tag{2}$$

Using a polar representation of the two "sites", namely $a = A\mathrm{e}^{\mathrm{i}\theta_a}$, $b = B\mathrm{e}^{\mathrm{i}\theta_b}$, we immediately obtain $\sin\theta = 0$, where $\theta = \theta_b - \theta_a$, and hence the resulting equations for the amplitudes are

$$EA = \pm kB + A^3, \quad EB = \pm kA + B^3. \tag{3}$$

The simpler solutions of the above system are symmetric ones of amplitudes $A^2 = B^2 = E \mp k$ with the upper (lower) sign corresponding to the in-phase (out-of-phase) profile. In addition, there exist asymmetric solutions of amplitudes $A \neq B$, which can be determined by the following equations derived by eliminating E from (3):

$$AB = \pm k, \quad A^2 + B^2 = E\,. \tag{4}$$

The amplitudes $A^2 = (E \pm \sqrt{E^2 - 4k^2})/2$, $B = k/A$, exist *only* for $E^2 > 4k^2$ and thus for $E > 2k$ or $E < -2k$. These asymmetric solutions coincide with the symmetric ones at $E^2 = 4k^2$, and hence a *pitchfork* symmetry-breaking bifurcation is responsible for their emergence in the nonlinear problem. As is known from previous works [5, 11, 12], this bifurcation arises for the focusing (attractive) nonlinearity case $k > 0$ at the point $E = 2k$, and does so from the symmetric branch. However, in the defocusing (repulsive) case $k < 0$ the bifurcation arises when $E = -2k$ and the asymmetric solution emerges from the antisymmetric branch. This bifurcation picture is also complemented by the stability eigenvalues for the focusing and defocusing cases below (see Sec. 2.2).

2.2. PT-SYMMETRIC DNLS DIMER

We now turn to the PT-symmetric variant of the DNLS dimer, as it was recently analyzed in Ref. [28] (see also Ref. [22] for the experimental investigation of Ref. [20]). This setting is described by the system

$$\begin{aligned} \mathrm{i}\frac{\mathrm{d}u_1}{\mathrm{d}t} &= -ku_2 - |u_1|^2 u_1 - \mathrm{i}\gamma u_1, \\ \mathrm{i}\frac{\mathrm{d}u_2}{\mathrm{d}t} &= -ku_1 - |u_2|^2 u_2 + \mathrm{i}\gamma u_2, \end{aligned} \tag{5}$$

which incorporates matched linear loss and gain of strength γ acting on the components u_1 and u_2. The stationary equations have the form

$$Ea = kb + |a|^2 a + \mathrm{i}\gamma a\,, \quad Eb = ka + |b|^2 b - \mathrm{i}\gamma b\,. \tag{6}$$

Using the same polar decomposition as before, we find that the amplitudes and phase difference of the symmetric solutions satisfy

$$A^2 = B^2 = E \pm \left(k^2 - \gamma^2\right)^{1/2}, \tag{7}$$

$$\sin\theta = -\gamma/k\,, \tag{8}$$

where the signs in (7) correspond to the first (+) and second (-) branches. These two solutions exist *only* up to $\gamma = k$, while there is no such limit in the Hermitian case $\gamma = 0$. The latter is the critical threshold for the PT symmetry breaking of the underlying linear problem, whose eigenvalues are $E = \pm\left(k^2 - \gamma^2\right)^{1/2}$. Beyond this

critical value the eigenvalues become imaginary. Additionally, as is shown in Ref. [28], the stability eigenvalues of this PT-symmetric dimer are

$$\pm 2\mathrm{i}\left[2(k^2-\gamma^2)-E\left(k^2-\gamma^2\right)^{1/2}\right]^{1/2}$$

for the (–) branch, and

$$\pm 2\mathrm{i}\left[2(k^2-\gamma^2)+E\left(k^2-\gamma^2\right)^{1/2}\right]^{1/2}$$

for the (+) branch.

For the case $\gamma=0$ (see Sec. 2.1), these eigenvalues describe the critical value of E, where the two branches become unstable, and the pitchfork bifurcation leading to the asymmetric states emerges. Specifically, if $k>0$ (focusing nonlinearity), the first branch corresponding to the symmetric solutions becomes unstable at $E=2k$; if $k<0$ (defocusing nonlinearity), the destabilization arises when $E=-2k$, and this happens for the second branch corresponding to the antisymmetric branch $\theta=\pi$.

Similar stability conclusions occur for $\gamma\neq 0$, where only the (–) branch becomes unstable, but now also for $\gamma^2\geq k^2-E^2/4$. This suggests that there are two possibilities. If the propagation constant E (and the coupling strength k) are such that $E^2<4k^2$, then the instability is induced by the increase of the PT-symmetry parameter γ at the critical point. However, if $E^2>4k^2$, the instability has "already" taken place due to the presence of nonlinearity, and the (-) branch is unstable even in the $\gamma=0$ limit. In the latter case the presence of the gain-loss aspect only enhances the instability.

What has become of the pitchfork bifurcation picture explored earlier? We can see that the same instability is present here (at least if $E^2>4k^2$). However, analogs of the symmetry-broken states past the critical point, *i.e.*, stationary asymmetric states (emerging after the instability of the symmetric states), cannot be identified. Inevitably, the question of their fate arises. This type of question was initially raised in Ref. [19] (where a leaky quantum dimer, with loss only, was considered) and, past a critical point, states with a complex (instead of real) "eigenvalue" E were identified. In the PT-symmetric context, a similar idea was put forth in Ref. [38] for a double well consisting of two delta functions. In our paper we unify the approaches of Refs. [19, 38] by computing the "ghost states" (as we characterize them) that emerge from the symmetry-breaking bifurcation.

Before presenting the computation of the ghost states, we comment that these states with complex (nonlinear) eigenvalue E are no longer *true* solutions of the original system (5). This is because of the U(1) invariance of the system, which

only allows stationary solutions with real E [so that $\left|\exp(\mathrm{i}Et)\right|^2 = 1$]. When this symmetry is violated, the solutions may satisfy the stationary equations (6), but are only ghost states of the original dynamical system because they do not satisfy (5). Thus, at best one expects that the dynamics may stay close to the dynamics of these ghost states, especially during the evolution of the symmetry-breaking instability. We return to this topic later.

To identify these stationary solutions, we introduce polar coordinates $E \to \exp(\mathrm{i}\phi_E)$ and get

$$\begin{aligned} EA\cos(\phi_E) &= kB\cos\theta + A^3 \\ EB\cos(\phi_E) &= kA\cos\theta + B^3, \end{aligned} \tag{9}$$

$$\begin{aligned} E\sin(\phi_E) &= k\frac{B}{A}\sin\theta + \gamma, \\ E\cos(\phi_E) &= -k\frac{A}{B}\cos\theta - \gamma. \end{aligned} \tag{10}$$

To derive the asymmetric ($A \neq B$) solutions, we rewrite these equations as

$$\begin{aligned} \cos\theta &= AB/k, \\ \sin\theta &= -\frac{2\gamma}{k}\frac{AB}{A^2+B^2}, \end{aligned} \tag{11}$$

$$\begin{aligned} E\cos(\phi_E) &= A^2 + B^2, \\ E\sin(\phi_E) &= \gamma\frac{A^2 - B^2}{A^2 + B^2}. \end{aligned} \tag{12}$$

Applying the identity $\sin^2\chi + \cos^2\chi = 1$ to (11), we obtain a condition for the solution amplitudes, and the same identity applied to (12) yields the parameter E. These solutions exist *only* for $\gamma^2 > k^2 - E^2/4$. If $E^2 > 4k^2$, they exist for all values of γ (i.e., they have bifurcated "already" due to the nonlinearity). Also, these solutions terminate as $\theta \to -\pi/2, \quad \phi_E \to \pi/2$. In turn, this implies that in this limit both B and A vanish, with the ratio between them having the limit $B/A \to (\gamma \pm \sqrt{\gamma^2 - k^2})/k$. Thus, we have identified the disappearance point $\gamma^2 = E^2 + k^2$ of these symmetry-broken solutions.

Finally, we discuss the disappearance of the two symmetric states at the critical point $\gamma = k$, which is the phase-transition point of the linear (and nonlinear) problem. We have shown that at this point the symmetry-broken states still exist, but that now they are only ghost states of the steady-state problem. From the point

of view of nonlinear theory, one may be content to find a saddle-center bifurcation at this point, which leads to the disappearance of these solutions as stationary states of the nonlinear problem. Yet, once again, when these solutions disappear (even in the normal form of such a bifurcation) this means that they appear somewhere else within the complex plane of solutions. In order to compare this result with the linear PT-symmetric case, where the eigenvalues collide, become complex, and continue to exist in the complex plane, we follow Ref. [38] and consider the analytic continuation of our solutions. In the PT-symmetric regime up to the critical point, the solutions are chosen so that $u^*(x) = u(-x)$. (This is a broader statement for a spatially distributed system; in our simpler dimer setting, we need only replace x by the subscript *1* and $-x$ by the subscript *2*, or vice-versa.) Thus, to perform the analytic continuation, we use $u_j^* = u_{3-j}$ in (5), which leads to (9–10), but in the first pair of equations A^3 and B^3 are replaced by A^2B and B^2A. The result is

$$\xi = \frac{B}{A} = \frac{\gamma \pm \sqrt{\gamma^2 - k^2}}{k},$$
$$A^4 = \frac{E^2 - \gamma^2 \left(\dfrac{1-\xi^2}{1+\xi^2} \right)^2}{\xi^2}, \tag{13}$$

$$E \sin\left(\Phi_E\right) = \gamma \frac{1-\xi^2}{1+\xi^2} = \pm\sqrt{\gamma^2 - k^2}, \tag{14}$$
$$\theta = -\pi/2.$$

Note that the pitchfork symmetry-breaking branches also tend to this solution, as shown above in the expression for *B*/*A* in the limit of termination of the branch when $\gamma^2 = E^2 + k^2$. We have made an additional subtle assumption here, namely, that $\theta_a + \theta_b = 0$. We can obtain more general solutions without this assumption, but these do not appear to introduce new features to the problem.

The solutions stemming from the analytic continuation provide a complete description of the states of the system. We move from symmetric/antisymmetric states to asymmetric ones (which may be ghost states) through a pitchfork bifurcation, destabilizing the symmetric (antisymmetric) branch for a focusing (defocusing) nonlinearity. We terminate at the point of the linear PT phase transition, where the nonlinear eigenvalues of the symmetric branches collide and become complex, giving rise to an analytic continuation of our solutions in the complex plane. All solutions terminate at $\gamma^2 = k^2 + E^2$.

3. FROM THE NLS EQUATION WITH A DOUBLE-WELL POTENTIAL TO THE DIMER

The central problem of interest here is an NLS equation with a double-well potential,

$$\mathrm{i}u_t = Lu + \mathrm{i}V_{\mathrm{PT}}u + |u|^2 u, \tag{15}$$

where $u_t = \partial u / \partial t$. Here, $u(x,t)$ is a complex field (which can represent the electric field envelope in optics or the macroscopic wavefunction in BECs); $L = -(1/2)\partial_x^2 + V_{real}(x)$ is a linear Schrödinger operator containing a real, symmetric double-well potential $V_{real}(x)$ (see, e.g., Refs. [5, 12]); iV_{PT} is a purely imaginary odd potential with $V_{\mathrm{PT}}(-x) = -V_{\mathrm{PT}}(x)$.

3.1. TWO-MODE REDUCTION

In such settings two-mode approximations have been valuable tools for studying the statics, stability, and dynamics of the system (see rigorous justifications in Refs. [43-45]). However, we do not use a Galerkin truncation to the ground and excited eigenmodes $\{u_0, u_1\}$ of the linear operator L with eigenvalues ω_0, ω_1 [12, 11, 43, 44, 45], but rather the rotated basis $\{u_L, u_R\}$ [5, 46]

$$u_L = (u_0 - u_1)/\sqrt{2}, \quad u_R = (u_0 + u_1)/\sqrt{2}. \tag{16}$$

The subscripts L and R denote the left and right well of V_{real}. Note that u_0 and u_1 (the ground- and first-excited state) are even and odd functions of x.

Following Ref. [46], we approximate the solution of (7) by the Galerkin expansion $u(x,t) = c_L(t)u_L(x) + c_R(t)u_R(x)$, where $c_{L,R}$ are unknown time-dependent coefficients. Substituting this ansatz into (7) and subsequently projecting on u_L, u_R, we obtain the following equations for $c_{L,R}$:

$$\begin{aligned} \mathrm{i}\frac{\mathrm{d}c_L}{\mathrm{d}t} &= \Omega c_L - \omega c_R + \mathrm{i}\gamma_L c_L + \eta_L |c_L|^2 c_L, \\ \mathrm{i}\frac{\mathrm{d}c_R}{\mathrm{d}t} &= \Omega c_R - \omega c_L + \mathrm{i}\gamma_R c_R + \eta_R |c_R|^2 c_R, \end{aligned} \tag{17}$$

where $\Omega = (\omega_0 + \omega_1)/2$ and $\omega = (\omega_1 - \omega_0)/2$. Also, $\gamma_{L,R} = \int \mathrm{d}x\, V_{\mathrm{PT}}(x) u_{L,R}^2$, and due to the parities of $u_{0,1}$ and V_{PT} it follows that $\gamma_L = -\gamma_R \equiv \gamma$. To derive the system above we have assumed, in addition to the truncation itself, that the overlap

integrals $\int \mathrm{d}x\, \Phi_L^2\, \Phi_R^2$, $\int \mathrm{d}x\, \Phi_L^3\, \Phi_R$, and $\int \mathrm{d}x\, \Phi_R^3\, \Phi_L$ are negligible in comparison to $\eta_L \equiv \int \mathrm{d}x\, \Phi_L^4$ and $\eta_R \equiv \int \mathrm{d}x\, \Phi_R^4$. This approximation becomes better as the distance between the wells becomes larger because these three integrals depend exponentially on the separation between the wells because of the exponential decay of the bound states $u_{L,R}(x)$. (Comparisons of these terms with the dominant terms η_L, η_R can be found in Ref. [46], which attests to the validity of this approximation.) Note that, as shown in Ref. [12], even the full model with these additional terms is analytically tractable. However, for our present purposes, this assumption considerably simplifies the analysis and helps to connect with the study of the PT-symmetric DNLS dimer. The equality $\eta_L = \eta_R \equiv \eta$ mirrors the symmetric nature of $V_{real}(x)$, while $\gamma_L = -\gamma_R \equiv \gamma$, mirrors the antisymmetric nature of $V_{\mathrm{PT}}(x)$.

We now consider solutions to (9) of the form

$$c_{L,R}(t) = \eta^{-1/2} C_{L,R} \exp(-\mathrm{i}\mu t), \tag{18}$$

where $C_{L,R}$ are unknown constant amplitudes and μ is the propagation constant (chemical potential in BECs). The prefactor $\eta^{-1/2}$ is used to rescale the term in front of the nonlinearity. Substituting this ansatz into (9) and using $E = \mu - \Omega$ as the (nonlinear) eigenvalue, we find that $C_{L,R}$ satisfy precisely the stationary equations for the DNLS PT-symmetric dimer

$$\begin{aligned} EC_L &= kC_R + |C_L|^2 C_L + \mathrm{i}\gamma C_L, \\ EC_R &= kC_L + |C_R|^2 C_R - \mathrm{i}\gamma C_R, \end{aligned} \tag{19}$$

where we have used the notation $-\omega = k$.

To further justify our assumptions regarding the overlap integrals, we note that for the Hamiltonian case of $\gamma = 0$, the symmetry breaking is predicted to occur at $E = \mu - \Omega = 2k = -2\omega$ for the focusing nonlinearity case and at $\mu - \Omega = -2k = 2\omega$ for the defocusing one. This implies a bifurcation at $\mu = (3\omega_0 - \omega_1)/2$ in the focusing case and at $\mu = (3\omega_1 - \omega_0)/2$ in the defocusing case. The corresponding predictions for the bifurcations induced by nonlinearity for (15) are $\mu = \omega_0 - A_0(\omega_1 - \omega_0)/(3B - A_0)$ for the focusing case, while the critical μ for the defocusing one is $\mu = \omega_0 + 3B(\omega_1 - \omega_0)/(3B - A_1)$ [12]. In these expressions $A_0 = \int \mathrm{d}x\, u_0^4$, $A_1 = \int \mathrm{d}x\, u_1^4$, while $B = \int \mathrm{d}x\, u_0^2 u_1^2$. Hence, it is clear that the approximation for the overlap integrals made above is tantamount to

$A_0 = A_1 = B$ because in that case the two expressions (the one from the dimer and the one from the exact two-mode reduction) coincide, showing that this is a reasonable approximation and that it trades a simple prediction for the critical points, which can be quantified just by knowing the eigenvalues of the underlying linear problem, for a small loss of accuracy in the result. This is the approximation that we use for the full problem.

3.2. DIRECT SIMULATIONS *VERSUS* ANALYTICAL APPROXIMATIONS

Having reduced (15) to the simple dimer model of (19), we now use the results of Sec. 2 to study the bifurcations of our PT-symmetric NLS model. To make connections between our work and earlier papers on double-well potentials, we use the same form of the double-well potential that was used in Refs. [12, 46]. It should, however, be evident from the exposition above that our basic phenomenology and corresponding conclusions will be quite general. In particular, we consider a potential of the form $V(x) = V_{real}(x) + iV_{PT}(x)$, where

$$V_{real}(x) = \frac{1}{2}\Omega_{tr}^2 x^2 + V_0 \sec h^2\left(\frac{x}{w}\right),$$
$$V_{PT}(x) = \varepsilon x \exp\left(-\frac{x^2}{2}\right). \tag{20}$$

The real (even) potential $V_{real}(x)$ consists of a parabolic trap of strength Ω_{tr} and a localized barrier potential of strength V_0 and width w, which has a standard double-well structure (that is easily achievable, e.g., in atomic BECs). The imaginary potential $V_{PT}(x)$ of strength ε has a prototypical antisymmetric gain-loss profile [42]. Hereafter, we fix the parameters of V_{real} to be $\Omega_{tr} = 0.1$, $V_0 = 1$ and $w = 0.5$, which yields the two lowest eigenvalues of the potential as $\omega_0 = 0.13282$ and $\omega_1 = 0.15571$. This imposes a tunneling strength between the wells of $k = -0.01145$.

There are now two possible paths to follow, both of which yield the symmetry-breaking pitchfork bifurcation, as indicated above. The first involves increasing the propagation constant μ (and hence the dimer eigenvalue E), thus increasing the strength of the nonlinearity. The second involves increasing the PT-symmetric potential parameter ε (and hence the corresponding dimer parameter γ). Both of these paths will yield the pitchfork bifurcation when $\gamma^2 = k^2 - E^2/4$ if the nonlinearity is sufficiently weak (namely, $E^2 < 4k^2$). However, only the latter path, which we follow below, exhibits the PT -symmetry-breaking phase transition when $\gamma = \pm k$.

In Fig. 1 we show the bifurcation diagram $N = N(\gamma)$, where $N = \int_{-\infty}^{\infty} \mathrm{d}x |u|^2$ represents the energy in optics (number of atoms in BECs). The figure compares the full PDE model with the PT-symmetric dimer model, where the real part of the chemical potential is chosen to be $\mu = 0.16$. This choice of μ is justified by the requirement to be sufficiently close to the linear eigenvalues so that the two-mode picture is valid. Given the defocusing nature of the nonlinearity used, $\mu > \omega_1$. A focusing variant of the problem was studied in Ref. [38]; based on our comments in the previous sections, it is easy to adapt the results below (upon the exchange of the antisymmetric branch with the symmetric branch as the parent branch in the pitchfork bifurcation).

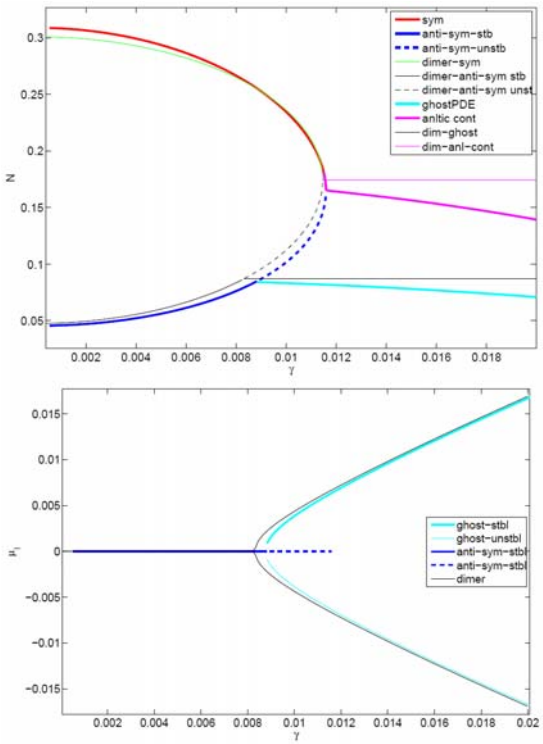

Fig. 1 – (Color online). Top panel: Bifurcation diagram $N = N(\gamma)$. The thin lines are the predictions of the two-mode analysis (the solid line denotes a linearly stable branch, while the dashed line depicts a linearly unstable one). The thick lines represent the full PDE analog (with the same s tability designation). Bottom panel: Bifurcation diagram $\mu_I = \mu_I(\gamma)$. The emergence of the ghost branches is shown as a supercritical pitchfork bifurcation in these variables. Once again, a comparison to the two-mode picture is given; μ_I is computed according to the last equation of (12), leading to $\mu_I = \pm\gamma\sqrt{(\mu-\Omega)^2 + 4\gamma^2 - 4k^2}\,/\sqrt{(\mu-\Omega)^2 + 4\gamma^2}$.

There is a good agreement between the full PDE model and the DNLS dimer results despite the multiple approximations employed (from the original PDE to the two-mode system and then from the two-mode system to the dimer). The main features of the bifurcation diagram are as follows. For small values of γ there are only two states with real chemical potential corresponding to the symmetric and antisymmetric ones for $\gamma = 0$. These states are the top and the bottom one, respectively, coming from the limiting value $\gamma = 0$. As we approach the PT phase transition (by increasing γ), the symmetric branch develops an antisymmetric imaginary part (see top left panel of Fig. 2).

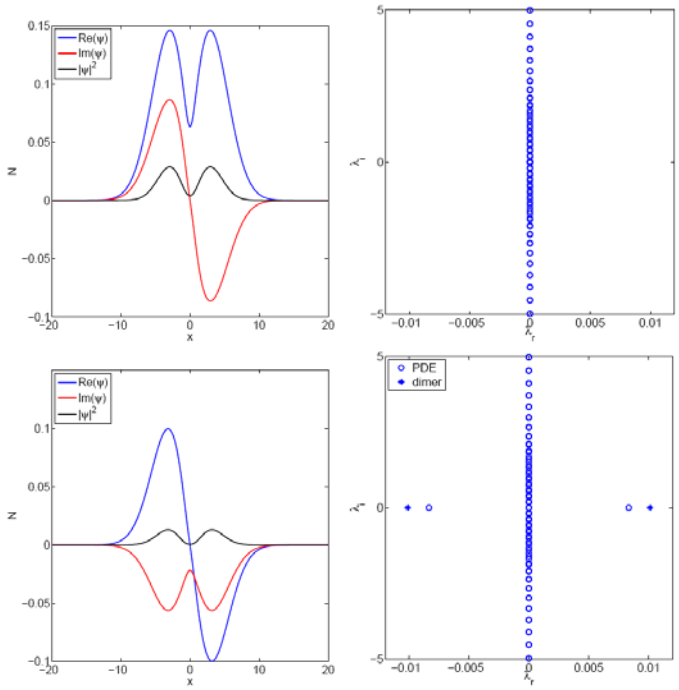

Fig. 2 – (Color online). Real and imaginary parts of the states with real (nonlinear) eigenvalues or equivalently real chemical potential. The left panel presents the real and imaginary parts of the states and their square modulus, while the right panel presents their corresponding eigenvalues of the linearization. The top panel is for the symmetric state, while the bottom is for the antisymmetric state. Both profiles are for the value of $\gamma = 0.0100$ for which the antisymmetric state is unstable. The two-mode prediction for the relevant instability eigenvalue is indicated by stars.

Conversely, the antisymmetric branch develops a symmetric imaginary part (see bottom left panel of Fig. 2). At the critical point the two waveforms are a $\pi/2$ rotation of one another; thus, they are functionally equivalent in our $U(1)$-invariant setting. These branches collide and disappear in the saddle-center bifurcation,

which is the nonlinear analog of the PT symmetry-breaking phase transition. The critical point for this transition is found to be at 0.01160 ± 0.00005 from the PDE, while it is at 0.01145 in the PT-symmetric dimer picture. Before this collision occurs, the antisymmetric state becomes unstable (turning into the saddle of the saddle-center bifurcation) at the critical point $\gamma = 0.0083 = \sqrt{k^2 - E^2/4}$. The corresponding symmetry-breaking bifurcation for the PDE occurs at $\gamma = 0.00888$. The result of this symmetry breaking in a purely nonlinear (non- PT symmetric) setting would have been the bifurcation of asymmetric states.

Asymmetric states arise as well, but these are the *ghost states* discussed above. These have been computed numerically and are shown in the top left panel of Fig. 3. A prototypical characteristic of these states, shown in the bottom panel of Fig. 1, is the imaginary part μ_I of the chemical potential μ of these states, which clearly demonstrates the pitchfork character of the bifurcation.

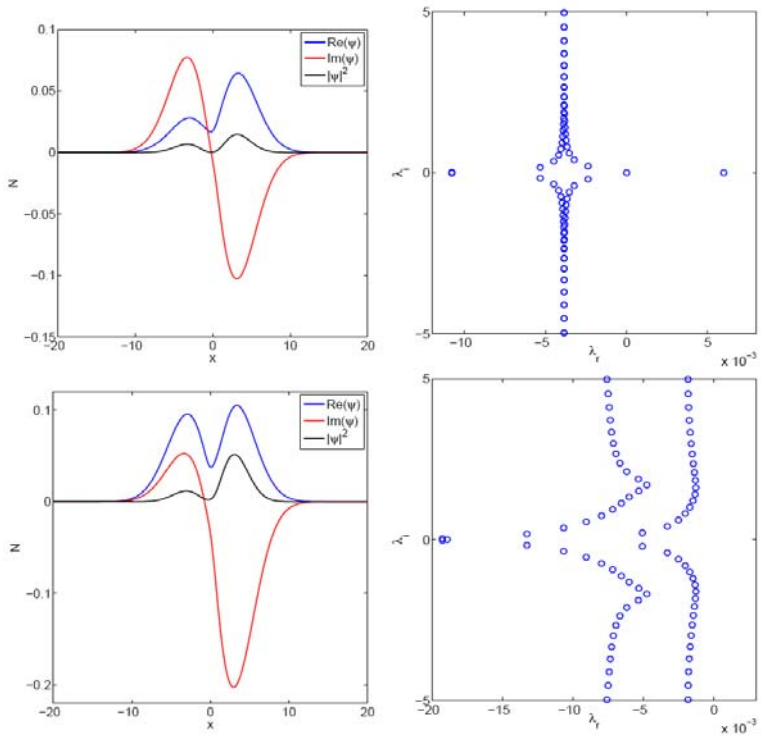

Fig. 3 – (Color online). Same as Fig. 2, but now the two states have an imaginary part in their chemical potential. The top panel corresponds to the profile (left) and the spectral plane of eigenvalues (right) for the ghost state stemming from the bifurcation given again at $\gamma = 0.0100$. The bottom panels, which closely resemble to the top ones, are for the state stemming from the analytic continuation computed for $\gamma = 0.0150$.

The parameter μ_I is self-consistently computed as follows. Recall that stationary solutions of (15), including the ghost solutions of complex μ, are governed by

$$\mu u = Lu + \mathrm{i}V_{\mathrm{PT}}u + |u|^2 u, \tag{21}$$

while the conjugate equation reads

$$\mu^* u^* = Lu^* - \mathrm{i}V_{\mathrm{PT}}u^* + |u|^2 u^*. \tag{22}$$

Then, multiplying (21) by u^* and (22) by u, integrating, and subtracting the second equation from the first, we obtain the self-consistency condition for the imaginary part μ_I of the chemical potential:

$$\mu_I = \frac{\int_{-\infty}^{\infty} \mathrm{d}x\, V_{PT}\, |u|^2}{\int_{-\infty}^{\infty} \mathrm{d}x\, |u|^2}. \tag{23}$$

This parameter corresponds to $E\sin(\phi_E)$ in the case of the dimer; that is, there is a direct analogy between (23) with (12), which becomes evident upon using the two-mode ansatz and the fact that $\gamma = \int \mathrm{d}x\, V_{PT}(x)\, u_L^2$. In this variable μ_I one can directly recognize the pitchfork nature of the bifurcation at $\gamma = 0.00888$ and the ghost nature of these states. In fact, only one of these is expected to survive (the one with positive μ_I, which leads to growth and is denoted in bold), while the one with negative μ_I decays and is not be observed in direct numerical simulations. These symmetry-broken states are mirror images of one another, but only one has the large amplitude at the "right" side (for $x > 0$, where there is indeed gain) (see the top panel of Fig. 3). The other state has the large amplitude at the "wrong" side (i.e., for $x < 0$, where there is loss).

The ghost states continue to exist past the critical point $\gamma = \pm k$ (as they are not subject to a bifurcation at that critical point). However, the other question is what becomes of the saddle and the center states (the former antisymmetric and former symmetric one) past the critical point of the PT phase transition. Following the suggestion of Ref. [38] and the fact that it is possible to require for both of the states with real μ (existing prior to the PT phase transition) that $u^*(x) = u(-x)$, we *enforce* this condition for $\gamma > k$. This provides for the original model an *analytic continuation* that is nonlocal in a highly nontrivial way; the steady-state equations read

$$\mu u(x) = Lu(x) + \mathrm{i}V_{VP}(x)u(x) + u^2(x)u(-x), \tag{24}$$

and there is cross talk of the field value at x and $-x$ within the nonlinear term. These states *fall back* on the original states for $\gamma < k$, but also provide their analytic continuation past this point. Interestingly, in this case, a new inner product is used to compute the energy (atom number) *N*. Given the substitution above, the energy now becomes $N = \int_{-\infty}^{\infty} \mathrm{d}x\, u(x)u(-x)$ (see also the review [2]). Also, from (23) we obtain

$$\mu_I = \frac{\int_{-\infty}^{\infty} \mathrm{d}x\; V_{PT}\; u(x)u(-x)}{\int_{-\infty}^{\infty} \mathrm{d}x\; u(x)u(-x)}\,. \tag{25}$$

The theoretical dimer predictions for the ghost branch and for the analytic continuation branch are also shown in terms of *N* as a function of γ in Fig. 1. In the former case of the ghost states, the normalized (based on the scaling transformation) norm is tantamount to $(A^2 + B^2)/\eta_L \equiv (\mu - \Omega)/\eta_L$,, which is a horizontal line shown in Fig. 1 bifurcating off of the theoretical point of $\gamma = 0.0083$. On the other hand, for the latter case of the analytic continuation states, we have $N = \int \mathrm{d}x\, u(x)u(-x) = 2c_L c_R = 2AB/\eta_L = 2(\mu - \Omega)/\eta_L$. While there is a slight decay of *N* in the PDE for both states, the result is close to the theoretical prediction of the dimer model. A similar weak dependence of a quantity similar to *N* on γ was observed in the focusing case [38].

Detailed examples of all branches are shown in Figs. 2–3. As described above, the symmetric branch shows a symmetric real part and an antisymmetric imaginary part, while the opposite occurs for the antisymmetric branch. Both branches are stable; up to the critical point no eigenvalues with positive real part arise. At that point, in the case of the antisymmetric branch, a pair of imaginary eigenvalues moves to the real axis (as shown in the bottom right panel of Fig. 2). The variation of the maximum real part of the eigenvalues of the antisymmetric branch as a function of γ is shown in Fig. 4. In both of the above panels the comparison with the analytical approximation given by $\lambda = \pm 2\mathrm{i}\left[2(k^2 - \gamma^2) - E\left(k^2 - \gamma^2\right)^{1/2}\right]^{1/2}$ is provided, which gives a measure of the agreement with the two-mode discrete picture.

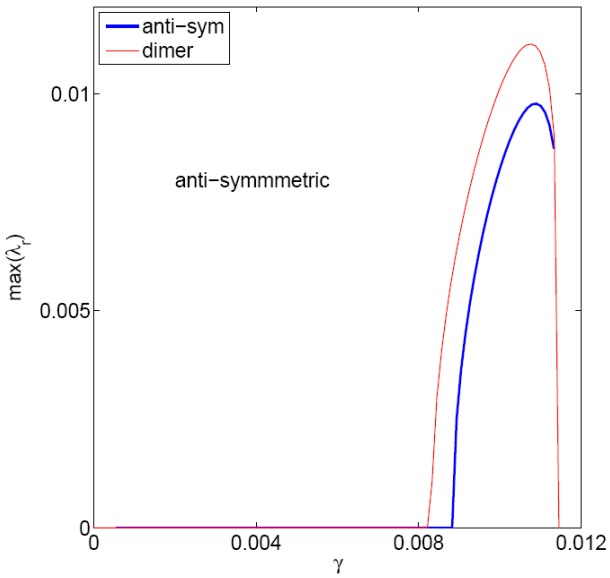

Fig. 4 – (Color online). Maximum value of the real part of the eigenvalues as a function of γ for the antisymmetric state. The instability sets in at $\gamma = 0.00888$; for comparison, the corresponding eigenvalue is also evaluated from the dimer reduction.

The eigenvalues of the ghost state that emerges from the supercritical pitchfork bifurcation are shown in the top right panel of Fig. 3. Here, the solution is unstable too, due to a positive real eigenvalue. Importantly, one also sees here a shift of neutrally stable eigenvalues to the left-half plane, where they lead to decaying excitations. This spectral picture is valid for the branch of positive μ_I. It should nevertheless be recalled that this stability analysis is not of direct use as these states are *not* stationary, and the existence of positive μ_I leads to an amplitude that grows in time. Similar conclusions can be drawn for the states resulting from the analytic continuation of the model. These states are presented in the bottom panel of Fig. 3; these states structurally resemble the ghost states, particularly in the profile of the square moduli. Although the model used to compute the latter is different and involves the nonlinearity $u^2(x)u(-x)$, both states have nonzero (positive in this case) μ_I, and both terminate at the same critical point as γ is increased in the two-mode analysis. This structural proximity of the profiles of the top and the bottom panel of Fig. 3 can be interpreted as a byproduct of the predicted proximity for large γ in the two-mode picture.

Finally, we studied the dynamics of the states by means of direct numerical simulations. Prior to the critical point, we examined the dynamical evolution of the instability of the antisymmetric state, as shown in Fig. 5 for $\gamma = 0.01090$. The top left panel illustrates a short time scale over which the mode becomes unstable. Note that the evolution of the antisymmetric mode between $t = 400$ and $t = 500$ closely emulates the growth of the ghost mode between $t = 0$ and $t = 100$. Its instability appears to follow the growth of the corresponding ghost mode, which is shown in the bottom left panel of Fig. 5. For longer time scales, the ghost mode itself becomes unstable and approaches another ghost state of the type that has been illustrated in Refs. [42, 47] (see the bottom right panel of Fig. 5). The latter state involves a dark soliton that has migrated to one of the wells of the double-well potential, accompanied by a growth of the amplitude and the width of the solution. Unfortunately, this type of state is intractable within the two-mode picture (as the latter does not allow for the possibility of intra-well dynamics). In the same way, the antisymmetric state, after transiting through its corresponding (for the same γ) ghost state, follows the instability and fate of the ghost state by forming for longer times the same tilted dark-soliton dynamical structure (see the top right panel of Fig. 5).

Having considered the dynamical instability prior to the PT phase transition critical point, we now turn to the dynamics of various states past the latter point of $\gamma = 0.01160$. Above the critical point (and, in particular, for $\gamma = 0.0150$) we performed the evolution of three different initial waveforms. The first initialization (whose evolution is shown in the left panel of Fig. 6) used the symmetric solution as obtained for a smaller value of γ, namely for $\gamma = 0.0100$, to examine the outcome of the "standard" waveforms past the PT-phase-transition point which leads to the termination of their existence. This dynamics illustrated a phenomenology similar to that shown earlier in Fig. 5. The initial growth stage was finally succeeded by the formation of a robust dark soliton on the left well of the potential. A similar evolution shown in the right panel of the figure was observed for the case of the ghost state with $\gamma = 0.0150$. We also performed a similar computation initialized with the result of the analytic continuation and a similar integration result was obtained (not shown). We conclude that past the critical point of the PT phase transition, the dynamics is typically attracted to dark soliton ghost states, which reside within the lossy well (and can thus not be captured by our two-mode picture).

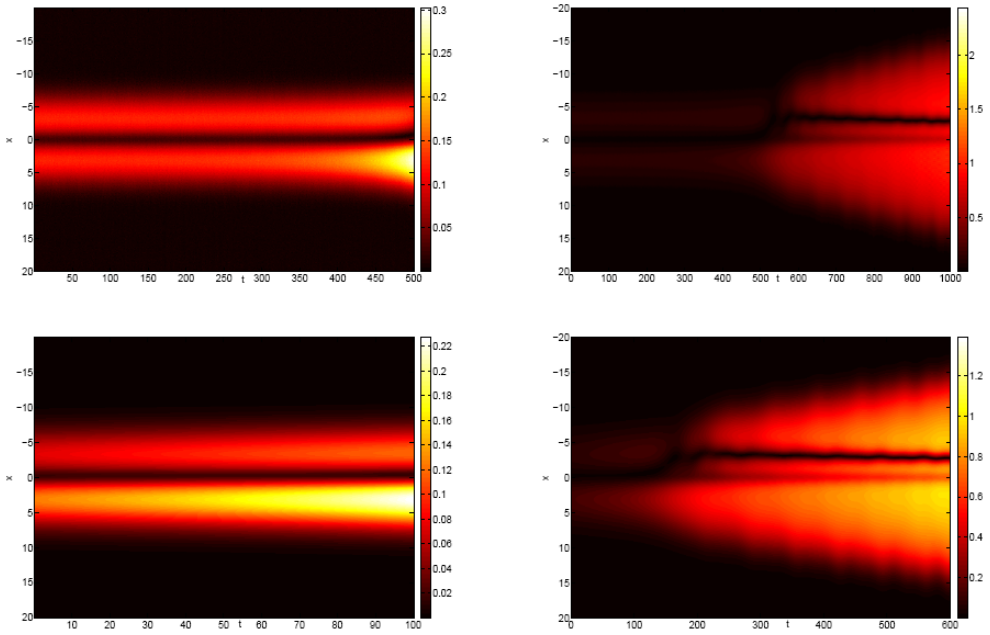

Fig. 5 – (Color online). Contour plots showing the space-time evolution of the density $|u(x,t)|^2$ (for $\gamma = 0.01090$). The top panels show the evolution of the antisymmetric state, illustrating its dynamical destabilization, and the bottom panels show the evolution of the ghost state. (Note the different time scales between the panels.) The left panels show early stages of the evolution (initial destabilization between $t = 0$ and $t = 400$ for the antisymmetric state and then growth from $t = 400$ to $t = 500$). The initial stage only shows the growth in the case of the ghost state enabled by positive μ_I. The right panels show the late stages of the evolution where dynamics, intractable within the two-mode model, develop. This evolution involves a dark-soliton state nucleated within the left well, similar to what was observed in Refs. [42,47].

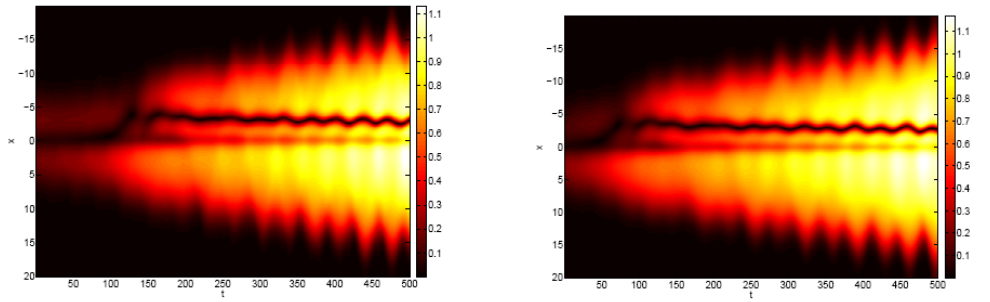

Fig. 6 – (Color online). Left panel: Space-time evolution of an exact solution of the symmetric branch obtained for $\gamma = 0.0100$, when initialized in (15) for $\gamma = 0.0150$, *i.e.*, past the critical point of the transition, where the symmetric branch no longer exists. Right panel: Evolution of the exact ghost state obtained for $\gamma = 0.0150$.

4. CONCLUSIONS AND OUTLOOK

In this paper we have used analytical and numerical methods to revisit the problem of a PT-symmetric double-well potential. We used a particular form for the symmetric real part and the antisymmetric (PT-symmetric) imaginary part of the potential, but we indicated that the specific choice of the potential is inconsequential. In fact, given the double-well structure and a suitable choice of parameters (such as the chemical potential, *i.e.*, the strength of the nonlinearity), one can reduce the problem to a two-mode regime. In that setting a reduction can be made explicit (and its assumptions/transformations can be suitably formulated) from the original PDE problem (the nonlinear Schrödinger model with a PT-symmetric double-well potential) to the simpler and analytically tractable dimer setting.

In the latter, we have shown that all characteristics of the system become transparent and we have identified the symmetric and antisymmetric states and their nonlinear continuation. We have quantified the pitchfork bifurcation, formerly leading to asymmetric states due to nonlinearity, and presently leading to ghost states due to PT-symmetry. We have explicitly obtained and monitored the daughter states of this bifurcation and their role in the dynamics, even though they are not exact solutions. We computed the PT phase transition (or simply the saddle-center bifurcation) of the two fundamental branches. Finally, the analytic continuation of the system past this critical point, with its unusual "nonlocal" (at least at the PDE level) cross talk of x and $-x$, was formulated. In all of the above, the analytics performed in the framework of the two-mode approximation remain invariably a reasonable approximation to the full original system and the numerical computations therein.

The above analysis gives a fundamental picture for the combined existence and interplay of nonlinearity, effective discreteness (through the double-well potential) and PT-symmetry. However, there are numerous directions for interesting generalizations of this work. One of these would be to consider the more complicated "oligomer" configurations of Ref. [28]; namely, the trimers and quadrimers (for the latter, see also Ref. [48] and even the plaquette two-dimensional building blocks of Ref. [49]). Another aspect that has emerged both here and in the context of Ref. [47] is to investigate the dynamics of the asymmetric states in which a dark soliton emerges and localizes within the lossy region. These are ghost states of the full PDE model; as we indicated, they cannot be captured by the two-mode approximation. These ghost states deserve a systematic investigation and classification. Generalizing to higher-dimensional settings, and introducing topologically charged states such as vortices [42, 47] would also be worth exploring. These topics are presently under study and results will be reported in future publications.

Acknowledgments. PGK gratefully acknowledges the support of the U.S. National Science Foundation under grants DMS-0806762 and CMMI-1000337, as well as the Alexander von Humboldt Foundation, the Alexander S. Onassis Public Benefit Foundation and the Binational Science Foundation. DJF was partially supported by the Special Account for Research Grants of the University of Athens. CMB is supported by the U.S. Department of Energy and the U.K. Leverhulme Foundation.

REFERENCES

1. C. M. Bender and S. Boettcher, Phys. Rev. Lett., **80**, 5243 (1998);
   C. M. Bender, S. Boettcher and P. N. Meisinger, J. Math. Phys., **40**, 2201 (1999).
2. C. M. Bender, Rep. Prog. Phys., **70**, 947 (2007).
3. M. Albiez, R. Gati, J. Fölling, S. Hunsmann, M. Cristiani, and M. K. Oberthaler, Phys. Rev. Lett., **95**, 010402 (2005).
4. T. Zibold, E. Nicklas, C. Gross, and M. K. Oberthaler, Phys. Rev. Lett., **105**, 204101 (2010).
5. S. Raghavan, A. Smerzi, S. Fantoni, and S. R. Shenoy, Phys. Rev. A, **59**, 620 (1999);
   S. Raghavan, A. Smerzi, and V. M. Kenkre, Phys. Rev. A, **60**, R1787 (1999);
   A. Smerzi and S. Raghavan, Phys. Rev. A, **61**, 063601 (2000).
6. E. A. Ostrovskaya, Yu. S. Kivshar, M. Lisak, B. Hall, F. Cattani, and D. Anderson, Phys. Rev. A, **61**, 031601(R) (2000).
7. K. W. Mahmud, J. N. Kutz, and W. P. Reinhardt, Phys. Rev. A, **66**, 063607 (2002).
8. V. S. Shchesnovich, B. A. Malomed, and R. A. Kraenkel, Physica D, **188**, 213 (2004).
9. D. Ananikian and T. Bergeman, Phys. Rev. A,**73**, 013604 (2006).
10. P. Ziń, E. Infeld, M. Matuszewski, G. Rowlands, and M. Trippenbach, Phys. Rev. A, **73**, 022105 (2006).
11. T. Kapitula and P. G. Kevrekidis, Nonlinearity, **18**, 2491 (2005).
12. G. Theocharis, P. G. Kevrekidis, D. J. Frantzeskakis, and P. Schmelcher, Phys. Rev. E, **74**, 056608 (2006).
13. D. R. Dounas-Frazer, A. M. Hermundstad, and L. D. Carr, Phys. Rev. Lett., **99**, 200402 (2007).
14. T. Mayteevarunyoo, B. A. Malomed, and G. Dong, Phys. Rev. A, **78**, 053601 (2008).
15. C. Paré and M. Florjańczyk, Phys. Rev. A **41**, 6287 (1990);
    A. I. Maimistov, Kvant. Elektron., **18**, 758 (1991) [Sov. J. Quantum Electron. **21**, 687 (1991)];
    W. Snyder, D. J. Mitchell, L. Poladian, D. R. Rowland, and Y. Chen, J. Opt. Soc. Am. B, **8**, 2102 (1991);
    P. L. Chu, B. A. Malomed, and G. D. Peng, J. Opt. Soc. Am. B, **10**, 1379 (1993);
    N. Akhmediev and A. Ankiewicz, Phys. Rev. Lett., **70**, 2395 (1993);
    B. A. Malomed, I. Skinner, P. L. Chu, and G. D. Peng, Phys. Rev. E, **53**, 4084 (1996).
16. C. Cambournac, T. Sylvestre, H. Maillotte , B. Vanderlinden, P. Kockaert, Ph. Emplit, and M. Haelterman, Phys. Rev. Lett., **89**, 083901 (2002).
17. P. G. Kevrekidis, Z. Chen, B. A. Malomed, D. J. Frantzeskakis, and M. I. Weinstein, Phys. Lett. A, **340**, 275 (2005).
18. A. Ruschhaupt, F. Delgado, and J.G. Muga, J. Phys. A: Math. Gen., **38**, L171 (2005);
    A. Guo, G. J. Salamo, D. Duchesne, R. Morandotti, M. Volatier-Ravat, V. Aimez, G. A. Siviloglou, and D. N. Christodoulides, Phys. Rev. Lett., **103**, 093902 (2009).
19. M. Hiller, T. Kottos, and A. Ossipov, Phys. Rev. A, **73**, 063625 (2006).
20. C. E. Rüter, K. G. Makris, R. El-Ganainy, D. N. Christodoulides, M. Segev, and D. Kip, Nature Phys., **6**, 192 (2010).
21. J. Schindler, A. Li, M. C. Zheng, F. M. Ellis, and T. Kottos, Phys. Rev. A, **84**, 040101 (2011).
22. H. Ramezani, T. Kottos, R. El-Ganainy, and D. N. Christodoulides, Phys. Rev. A, **82**, 043803 (2010).

23. A. A. Sukhorukov, Z. Xu, and Yu. S. Kivshar, Phys. Rev. A, **82**, 043818 (2010).
24. M. C. Zheng, D. N. Christodoulides, R. Fleischmann, and T. Kottos, Phys. Rev. A, **82**, 010103(R) (2010).
25. E. M. Graefe, H. J. Korsch, and A. E. Niederle, Phys. Rev. Lett., **101**, 150408 (2008).
26. E. M. Graefe, H. J. Korsch, and A. E. Niederle, Phys. Rev. A, **82**, 013629 (2010).
27. Z. Lin, H. Ramezani, T. Eichelkraut, T. Kottos, H. Cao, and D. N. Christodoulides, Phys. Rev. Lett., **106**, 213901 (2011).
28. K. Li and P. G. Kevrekidis, Phys. Rev. E, **83**, 066608 (2011).
29. S. V. Dmitriev, S. V. Suchkov, A. A. Sukhorukov, and Yu. S. Kivshar, Phys. Rev. A, **84**, 013833 (2011)
30. S. V. Suchkov, B. A. Malomed, S. V. Dmitriev, and Yu. S. Kivshar, Phys. Rev. E, **84**, 046609 (2011).
31. R. Driben and B. A. Malomed, Opt. Lett., **36**, 4323 (2011).
32. R. Driben and B. A. Malomed, Europhys. Lett., **96**, 51001 (2011).
33. F. Kh. Abdullaev, V.V. Konotop, M. Ögren and M. P. Sørensen, Opt. Lett., **36**, 4566 (2011).
34. N.V. Alexeeva, I.V. Barashenkov, A.A. Sukhorukov, and Yu.S. Kivshar, Phys. Rev. A, **85**, 063837 (2012).
35. A. E. Miroshnichenko, B. A. Malomed, and Yu. S. Kivshar, Phys. Rev. A, **84**, 012123 (2011).
36. F. Kh. Abdullaev, Y. V. Kartashov, V. V. Konotop, and D. A. Zezyulin, Phys. Rev. A, **83**, 041805 (2011);
    L. Chen, R. Li, N. Yang, D. Chen, L. Li, Proc. Romanian Acad. A, **13**, 46 (2012);
    Y. J. He, X. Zhu, D. Mihalache, J. L. Liu, and Z. X. Chen, Phys. Rev. A, **85**, 013831 (2012);
    Y. He, X. Zhu, D. Mihalache, J. Liu, and Z. Chen, Opt. Commun., **285**, 3320 (2012);
    Y. J. He and D. Mihalache, Rom. Rep. Phys., **64**, 1243 (2012).
37. D. A. Zezyulin, Y. V. Kartashov, and V. V. Konotop, Europhys. Lett., **96**, 64003 (2011).
38. H. Cartarius and G. Wunner, Phys. Rev. A, **86**, 013612 (2012);
    H. Cartarius, D. Haag, D. Dast, and G. Wunner, J. Phys. A: Math. Theor., **45**, 444008 (2012).
39. V. M. Kenkre and D. K. Campbell, Phys. Rev. B, **34**, 4959 (1986).
40. E.-M. Graefe, J. Phys. A: Math. Theor., **45**, 444015 (2012).
41. D. Dast, D. Haag, H. Cartarius, G. Wunner, R. Eichler, J. Main, Fortschritte der Physik, in press; doi:10.1002/prop.201200080, (2012).
42. V. Achilleos, P. G. Kevrekidis, D. J. Frantzeskakis, and R. Carretero-González, Phys. Rev. A, **86**, 013808 (2012).
43. E. W. Kirr, P. G. Kevrekidis, E. Shlizerman, and M. I. Weinstein, SIAM J. Math. Anal., **40**, 566 (2008).
44. J. L. Marzuola and M. I. Weinstein, Discr. Cont. Dyn. Sys., **28**, 1505 (2010).
45. E. Kirr, P. G. Kevrekidis, and D. E. Pelinovsky, Comm. Math. Phys., **308**, 795 (2011).
46. C. Wang, P. G. Kevrekidis, D. J. Frantzeskakis, and B. A. Malomed, Physica D, **240**, 805 (2011).
47. V. Achilleos, P. G. Kevrekidis, D. J. Frantzeskakis, and R. Carretero-González, preprint.
48. D. A. Zezyulin and V. V. Konotop, Phys. Rev. A, **85**, 043840 (2012); Phys. Rev. Lett., **108**, 213906 (2012).
49. K. Li, P.G. Kevrekidis, B. A. Malomed, and U. Guenther, J. Phys. A: Math. Theor., **45**, 444021 (2012).